JOURNAL OF MATERIALS SCIENCE 37 (2002) 1121 – 1129

Thermal decomposition of bauxite minerals: infrared emission spectroscopy of gibbsite, boehmite and diaspore

J. T. KLOPROGGE, H. D. RUAN, R. L. FROST
Centre for Instrumental and Developmental Chemistry, Queensland University of Technology, 2 George Street, GPO Box 2434, Brisbane, Q 4001, Australia
E-mail: t.kloprogge@qut.edu.au

Infrared emission spectroscopy has been used to study the dehydroxylation behavior over the temperature range from 200 to 750°C of three major Al-minerals in bauxite: gibbsite (synthetic and natural), boehmite (synthetic and natural) and diaspore. A good agreement is found with the thermal analysis and differential thermal analysis curves of these minerals. Loss in intensity of especially the hydroxyl-stretching modes of gibbsite, boehmite and diaspore as function of temperature correspond well with the observed changes in the TGA/DTA patterns. The DTA pattern of gibbsite clearly indicates the formation of boehmite as an intermediate shown by a endotherm around 500°C. Dehydroxylation of gibbsite is followed by a loss of intensity of the 3620 and 3351 cm^{-1} OH-stretching bands and the corresponding deformation band around 1024 cm^{-1}. Dehydroxylation starts around 220°C and is complete around 350°C. Similar observations were made for boehmite and diaspore. For boehmite dehydroxylation was observed to commence around 250°C and could be followed by especially the loss in intensity of the bands around 3319 and 3129 cm^{-1}. The DTA pattern of diaspore is more complex with overlapping endotherms around 622 and 650°C. The dehydroxylation can be followed by the decrease in intensity of the OH-stretching bands around 3667, 3215 and 2972 cm^{-1}. Above 550°C only a single band is observed that disappears after heating above 600°C corresponding to the two endotherms around 622 and 650°C in the DTA. © *2002 Kluwer Academic Publishers*

1. Introduction

Bauxite deposits form the major source of aluminum in our industrial world. The major aluminum phases recognised in bauxites and laterites are gibbsite also known as hydrargillite (γ-$Al(OH)_3$), boehmite (γ-AlO(OH)), and diaspore (α-AlO(OH)). In addition other commonly observed phases are kaolinite, allophane, quartz, goethite, and haematite (see e.g. [1–3]). Gibbsite is the principal component in tropical bauxites formed in areas characterised by a hot rainy climate with alternating dry periods (monsoon). Bauxites with mainly boehmite seem to be more restricted to the subtropical areas (Mediterranean type bauxite). Thermal action or low-grade metamorphism mostly favours diaspore formation. Furthermore, diaspore is found as a minor constituent in many types of bauxite in addition to gibbsite and boehmite [4–6].

1.1. Structure of gibbsite, boehmite, and diaspore

Gibbsite is monoclinic ($P2_1/n$, $a = 5.0626$ Å, $b = 8.6719$ Å, $c = 9.4254$ Å, $\beta = 90.26°$) with mostly a tabular pseudohexagonal habit. The structure can be visualised as sheets of hcp layers with open packing between successive sheets. In the lateral extension of the hexagonal closed packed sheets each Al cation is octahedrally coordinated by 6 OH groups and each hydroxyl group is coordinated by two Al cations with one octahedral site vacant [7, 8]. This can also be visualised as double layers of OH groups with Al cations occupying two thirds of the interstices within the layers. Each double layer is positioned in such a way that the upper and lower neighbouring layers have their hydroxyl groups directly opposite to each other and not in the position of the closest packing. This type of layer structure explains the perfect cleavage of gibbsite parallel to the basal plane (001). Due to the superposition of the hydroxyl groups are the O–H bonds partially polarised causing displacement of the proton towards the vacant sites. Table I represents a short review on the structural parameters and the OH stretching and bending vibrations of gibbsite, boehmite and diaspore. Four stretching vibrations are observed in the range of 3620–3380 cm^{-1} in the infrared spectrum [6, 9]. Four OH bending vibrations are observed at 914, 969, 1020, and 1060 cm^{-1} corresponding to six independent sets of hydroxyls in the gibbsite structure [10]. Additional vibrations have been reported at 668, 560 and 450 cm^{-1} [6, 10].

TABLE I Structural data and OH stretching and bending frequencies of gibbsite, boehmite and diaspore

Compound	M . . . OH (Å)	OH . . . O(H) (Å)	ν(OH)				δ(OH)		γ(OH)			Reference
Gibbsite	1.73–2.14	2.75, 2.80, 2.82, 2.94	3617	3520	3428	3380	1020	958	914	802	743	[7, 11, 12]
Boehmite	1.87	2.70			3297	3090	1160	1080			755	[13, 14]
Diaspore	1.975–1.980	2.65			2994	2915	1077			963		[15–17]

Boehmite has the same structure as lepidocrocite (γ-FeO(OH)). The structure of boehmite consists of double layers of oxygen octahedra partially filled with Al cations [13]. Boehmite is orthorhombic with space group *Amam* ($a = 3.6936$ Å, $b = 12.214$ Å, $c = 2.8679$ Å) [8, 18]. The stacking arrangement of the three oxygen layers is such that the double octahedral layer is in cubic closed packing. Within the double layer one can discriminate between two different types of oxygen. Each oxygen in the middle of the double layer is shared by four other octahedra, while the oxygens on the outside are only shared by two octahedra. These outer oxygens are hydrogen-bonded to two other similarly coordinated oxygens in the neighbouring double layers above and below. The stacking of the layers is such that the hydroxyl groups of one layer are located over the depression between the hydroxyl groups in the adjacent layer. The IR spectrum of boehmite has a characteristic OH stretching band with two equally strong maxima at 3297 and 3090 cm^{-1} according to Ryskin [9]. Van der Marel and Beutelspacher [6] however reported a very strong maximum at 3280–3287 cm^{-1} and a very strong maximum at 3090 cm^{-1}. The enormous splitting has been ascribed to the presence of a direct bonding between the equivalent hydroxyls and to the high structural regularity of the structure. In the OH bending region boehmite is characterised by two vibrations at 1160 and 1080 cm^{-1}. The vibration at 755 cm^{-1} involves the hydrogen vibrations according to Fripiat *et al*. [14]. Van der Marel and Beutelspacher [6] report an additional vibration at 636 cm^{-1}.

Diaspore has a similar structure as goethite (α-FeO(OH)). In the case of diaspore the oxygens sheets are in hexagonal closed packing with two thirds of the octahedral sites filled with Al cations. The occupied octahedra are linked together by edge sharing forming double chains in the c-axis direction [15]. It is orthorhombic with space group *Pbnm* ($a = 4.4007$ Å, $b = 9.4253$ Å, $c = 2.8452$ Å) [8, 19]. Diaspore differs from boehmite in the coordination of the oxygen atoms, all of which are hydrogen-bonded to another oxygen. The hydrogens are closest to the oxygen farthest from the Al cation. This compact arrangement compared to boehmite explains the greater density and the low frequency of the OH stretching vibration shown by infrared absorption. The IR spectrum of diaspore clearly shows the influence of the crystal structure compared to boehmite. The shorter OH bonds and the lacking of direct bonding between the equivalent hydroxyl groups results in a shift of the OH stretching bends towards lower frequencies (2994 and 2915 cm^{-1}) and the splitting is strongly reduced to a value of approximately 70–80 cm^{-1} instead of the 200 cm^{-1} for boehmite. Van der Marel and Beutelspacher [6] report additional bands at 2115 and 2000 cm^{-1} (comparable to the 2128 and 1998 cm^{-1} reported in [9]). The OH bending region is characterised by two infrared active in-plane bending vibrations and one infrared active out-of-plane bending vibration around 1070–1080 cm^{-1} and 960–970 cm^{-1} respectively [6, 9, 16, 17].

1.2. Thermal decomposition of Al-phases in the Al_2O_3-H_2O system

The study of the thermal transformations of aluminium (oxy)hydroxides has resulted in many contradictory findings. Much of this is probably related to the experimental techniques and conditions used to determine these thermal transformations. The dehydroxylation of boehmite and gibbsite has been described as deceptively simple [20, 21]. The most stable member of the Al_2O_3-H_2O series is α-alumina. Linsen *et al*. make the point that most of the confusion arises from insufficient information about the reaction conditions [22]. The use of thermal techniques to study the dehydration and dehydroxylation of gibbsite has been widely documented [20]. It is clear that many variables must be taken into account when using techniques such as DTA, DSC, TGA, CRTA and quasi-isothermal TGA and isobaric TGA [22–24]. Such variables include heating rate, external pressure, water vapour pressure, sample particle size and even thickness of sample size in the DTA crucible [25].

The initial step in the thermal decomposition of gibbsite is the diffusion of protons and the reaction with hydroxyl ions to form water [23]. This process removes the binding forces between subsequent units in the gibbsite structure and causes changes in the chemical composition and density. Differential thermal analysis (DTA) of a coarse-grained gibbsite has shown the presence of an endotherm around 230°C followed by a second endotherm around 280°C [24]. This latter endotherm is attributed to the formation of boehmite via a hydrothermal reaction due to the retarded diffusion of water out of the larger gibbsite particles. This reaction was not observed in the DTA patterns of finely grained gibbsite. There is general agreement that boehmite and a disordered transition alumina (γ-alumina) are formed upon the thermal treatment of coarse gibbsite up to 400°C. However, when fine-grained gibbsite is rapidly heated, an X-ray amorphous product labelled ρ-alumina is obtained instead [26].

Diaspore easily dehydrates to α-alumina, while boehmite and gibbsite do not. This can be attributed to the similarities in the structures of α-alumina and diaspore, as both have hexagonal close packed structures,

whereas gibbsite and boehmite have cubic packed structures [27, 28]. Diaspore is considered to be a product of diagenetic weathering. Thus there is no apparent relationship of diaspore with the other alumina phases, which are generally formed by pedogenic weathering [29, 30]. Unless very high pressures are involved the formation of diaspore from boehmite is not possible.

There is much disagreement about the dehydroxylation (and dehydration) pathways of (pseudo) boehmite. It has been shown that under vacuum dehydroxylation of highly crystalline boehmite results in firstly the formation of γ-alumina followed by θ-alumina [31]. In contrast the dehydroxylation of poorly crystalline boehmite can follow two different pathways: 1) via amorphous Al_2O_3 to γ-alumina or 2) η-alumina to θ-alumina. Lippens and De Boer [32], in accordance with recent results by Ingram-Jones *et al*. [26], have suggested that between the γ and θ-aluminas δ-alumina is formed as an intermediate. Soled [33] has suggested that the γ-alumina actually contains a significant amount of amorphous material.

2. Experimental

2.1. Al (oxo) hydroxide samples

The aluminium phases used in this study are gibbsite from Minas Gerais, Brasil, collected by van der Marel (no. 11), synthetic gibbsite, natural boehmite from Hungary collected by van der Marel (no. 148), boehmite synthesised by P. Buining [34], and Mn-diaspore from Cape Provence, South Africa collected by van der Marel (no. 1151). Sjerry van der Gaast, NIOZ The Netherlands, kindly provided the samples collected by Van der Marel. The samples were analysed for phase purity by X-ray diffraction prior to the infrared emission spectroscopic analysis. X-ray diffraction has shown that the both the natural and synthetic gibbsites and the synthetic boehmite are pure. XRD of the Hungarian boehmite indicates traces of goethite, anatase and kaolinite or chlorite. The diaspore sample contains traces of talc and kaolinite. The diaspore from Cape Provence contains approximately 3% Mn but van der Marel and Beutelspacher [6] have shown that the infrared spectrum is similar to that of common diaspore. All samples were used without further purification.

2.2. Infrared emission spectroscopy

FTIR emission spectroscopy was carried out on a Digilab FTS-60A spectrometer, which was modified by replacing the IR source with an emission cell. A description of the cell and principles of the emission experiment have been published elsewhere [35]. Approximately 0.2 mg of the aluminum (oxo) hydroxide was spread as a thin layer on a 6 mm diameter platinum surface and held in an inert atmosphere within a nitrogen-purged cell during heating. The infrared emission cell consists of a modified atomic absorption graphite rod furnace, which is driven by a thyristor-controlled AC power supply capable of delivering up to 150 amps at 12 volts. A platinum disk acts as a hot plate to heat the aluminum (oxo) hydroxide sample and is placed on the graphite rod. An insulated 125-μm type R thermocouple was embedded inside the platinum plate in such a way that the thermocouple junction was $<$0.2 mm below the surface of the platinum. Temperature control of $\pm 2^{\circ}$C at the operating temperature of the aluminum (oxo) hydroxide sample was achieved by using a Eurotherm Model 808 proportional temperature controller, coupled to the thermocouple.

The design of the IES facility is based on an off axis paraboloidal mirror with a focal length of 25 mm mounted above the heater captures the infrared radiation and directs the radiation into the spectrometer. The assembly of the heating block, and platinum hot plate is located such that the surface of the platinum is slightly above the focal point of the off axis paraboloidal mirror. By this means the geometry is such that approximately 3 mm diameter area is sampled by the spectrometer. The spectrometer was modified by the removal of the source assembly and mounting a gold-coated mirror, which was drilled through the centre to allow the passage of the laser beam. The mirror was mounted at 45°, which enables the IR radiation to be directed into the FTIR spectrometer.

In the normal course of events, three sets of spectra are obtained: firstly the black body radiation over the temperature range selected at the various temperatures, secondly the platinum plate radiation is obtained at the same temperatures and thirdly the spectra from the platinum plate covered with the sample. Normally only one set of black body and platinum radiation is required. The emittance spectrum at a particular temperature was calculated by subtraction of the single beam spectrum of the platinum backplate from that of the platinum + sample, and the result ratioed to the single beam spectrum of an approximate blackbody (graphite). This spectral manipulation is carried out after all the spectral data has been collected.

The emission spectra were collected at intervals of 50°C over the range 200–750°C. The time between scans (while the temperature was raised to the next hold point) was approximately 100 seconds. It was considered that this was sufficient time for the heating block and the powdered sample to reach temperature equilibrium. The spectra were acquired by coaddition of 64 scans for the whole temperature range (approximate scanning time 45 seconds), with a nominal resolution of 4 cm^{-1}. Good quality spectra can be obtained providing the sample thickness is not too large. If too large a sample is used then the spectra become difficult to interpret because of the presence of combination and overtone bands. Spectral manipulation such as baseline adjustment, smoothing and normalisation was performed using the Spectracalc software package (Galactic Industries Corporation, NH, USA).

3. Results and discussion

In previous papers we have reported on the DTA/TGA analysis of a large number of selected gibbsite, boehmite and diaspore samples including those reported in this study [36–38]. The thermal analysis pattern depends on the origin of the sample, the impurities and the crystallinity of the sample. Fig. 1 gives an overview of the DTA patterns of the gibbsite, boehmite and diaspore

TABLE II Visible DTA endotherm maxima for gibbsite, boehmite and diaspore

Sample	Endotherm 1	Endotherm 2	Endotherm 3	Endotherm 4	Endotherm 5	Endotherm 6
Synthetic gibbsite	223°C		301°C	503°C		
Natural gibbsite 11		275°C	311°C	505°C		
Natural boehmite 148				502°C		
Natural diaspore 1151				532°C (very broad)	622°C	650°C

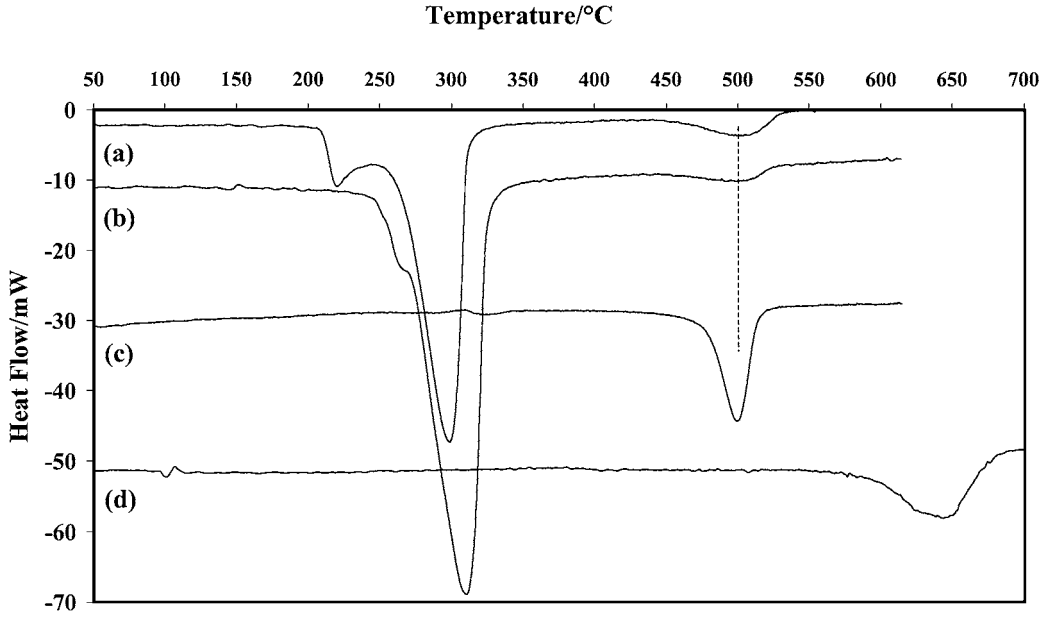

Figure 1 DTA patterns of (a) synthetic gibbsite, (b) natural gibbsite 11, (c) boehmite 148 and (d) diaspore 1151.

samples used in this study. The endotherm maxima are reported in Table II. The more highly crystalline gibbsites have endotherms at higher temperatures than the less crystalline ones. Each DTA endotherm is complex and shows several inflections. Clearly visible are the main endotherm around 300–310°C accompanied by a smaller endotherm at much lower temperature. This low temperature endotherm was attributed to non-hydrogen bonded 'outer' hydroxyl groups that are easily removed [36]. Published DTA patterns of a coarse-grained gibbsite show an endotherm centred on 230°C followed by a second at 280°C [24]. The latter endotherm was attributed to the formation of boehmite under hydrothermal conditions due to the retarded diffusion of water out of the larger gibbsite grains. A shallow endotherm may be observed between 500 and 550°C and is attributed to the dehydroxylation of the earlier formed boehmite.

The synthetic boehmite shows a substantial loss in weight at ~70°C due to the loss of water. The dehydroxylation around 300°C and is complete by 480°C. For the natural boehmite, the dehydroxylation starts at 480°C and is complete by 520°C. Analysis of the DTA pattern shows that the dehydroxylation pattern consists of a single endotherm around 502°C. The synthetic boehmite has been produced hydrothermally and consists of polymer-like fibrils. The natural boehmite is crystalline. Such difference in morphology may contribute to the differences in the observed temperatures of the dehydroxylation. It is concluded that the dehydroxylation is generally completed at 550°C.

Thermogravimetric analysis shows that diaspore loses 12% of its weight upon dehydroxylation over a short temperature range 500 to 530°C. The theoretical result for the decomposition $2AlO(OH) \rightarrow Al_2O_3 + H_2O$ is 15%. This result is in good agreement with previously published work [38]. A small weight loss (2%) over the temperature range from 100 to 200°C can be attributed to the loss of adsorbed water. The Mn substituted diaspore with 92% replacement of the Al shows two major endotherms at 622 and 650°C with a broad endotherm at 532°C. This broad endotherm corresponds with that previously observed for the non-substituted diaspore [38]. The TGA pattern of the Mn substituted diaspore shows a 12.5% weight loss commencing at 405°C with the major weight loss over the temperature range from 550 to 670°C. The effect of substitution of Mn for Al in the diaspore clearly stabilises the crystal structure of the diaspore as shown by the increased dehydroxylation temperature.

Fig. 2 shows the infrared absorption spectra of the gibbsite, boehmite and diaspore used in this study. The exact band positions are reported in Table III. Detailed descriptions of the infrared absorption spectra have been reported before by Frost and coworkers [36–38]. The infrared emission spectra are very similar but the bands are significantly broadened in comparison to the corresponding absorption spectra. This is a normal feature observed for infrared emission spectroscopy. Further in infrared emission spectra both the infrared active and Raman active bands will be observed. This also contributes to the width of the bands.

TABLE III Infrared absorption hydroxyl stretching and bending modes (cm^{-1}) for gibbsite, boehmite and diaspore

Compound	ν(OH)							δ(OH)					γ(OH)		
Synthetic gibbsite	3661	3620	3525	3452	3394	3375	3338	1059	1023	969	938				
Gibbsite 11		3621	3526	3460	3436	3377	3285	1054	1020	967	942	915			
Synthetic boehmite			3413		3283	3096	2977	1152	1081	1036	1012		749	635	542
Boehmite 148			3430		3275	3092	2931	1135	1071	1034	1007		748	626	539
Diaspore 1151		3446	3429	3270	3011	2923	2826	1086	1035	1007	966	914	751		

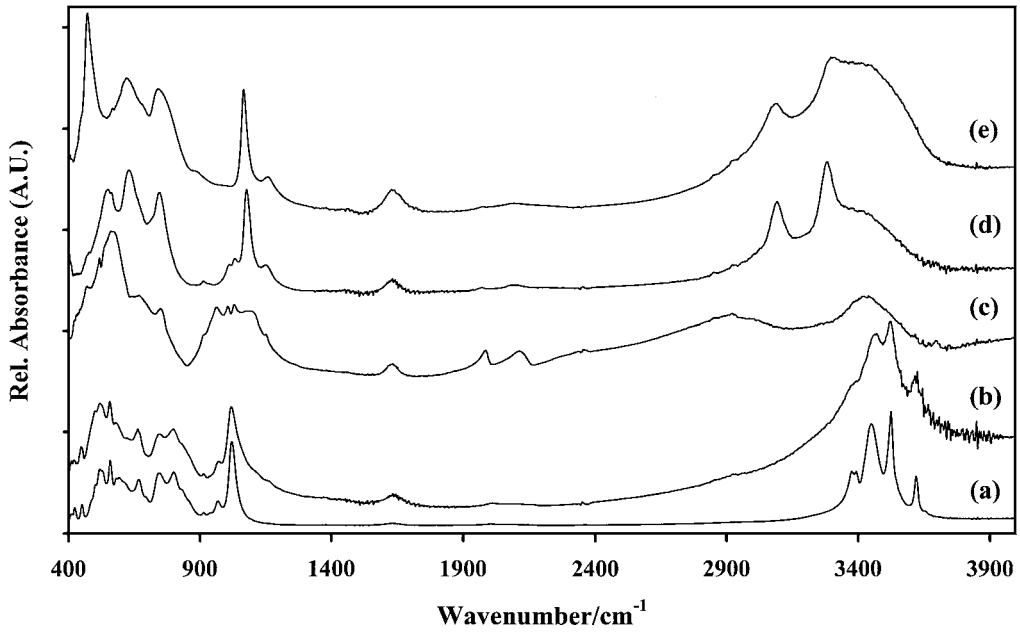

Figure 2 Infrared absorption spectra of (a) synthetic gibbsite, (b) natural gibbsite 11, (c) diaspore 1151, (d) natural boehmite 148 and (e) synthetic boehmite.

3.1. The hydroxyl stretching region

The infrared emission spectra of gibbsite, diaspore and boehmite are shown in Figs 3a–c respectively. As was observed in the absorption spectra, there are very little differences between the infrared emission spectra of the natural and synthetic gibbsites. Dehydroxylation of these three alumina phases can be observed by the decrease in intensity of the bands in the hydroxyl-stretching region (Fig. 4) and also by the decrease in intensity of the corresponding hydroxyl deformation modes. The infrared emission hydroxyl stretching bands of gibbsite overlap and are broad with little resolution. Band component analysis in the 200°C infrared emission spectra identified four hydroxyl-stretching modes at 3617, 3532, 3489 and 3351 cm^{-1}. This is in agreement with the four bands observed in the infrared absorption spectra. Furthermore, four crystallographically distinct hydroxyl groups can be identified in the structure of gibbsite. An earlier study has shown that three of the four hydroxyl stretching bands can observed at 3524, 3436 and 3365 cm^{-1} in the Raman spectra [36]. The first band at 3617 cm^{-1}, previously assigned to a non-hydrogen bonded hydroxyl shows a strong blue shift to 3626 cm^{-1} at 300°C and 3654 cm^{-1} at 350°C. The other three bands at 3532, 3489 and 3351 cm^{-1} show a red shift. For example the band at 3532 cm^{-1} at 200°C shifts to 3529 cm^{-1} at 300°C. The band at 3489 cm^{-1} shifts to 3381 cm^{-1} at 300°C. Similar blue and red shifts have also been observed for the inner hydroxyl groups and inner surface hydroxyls groups of kaolinite [39].

Fig. 3b displays the IES spectra of a synthetic boehmite. The spectra show the presence of organic chemicals as evidenced by the peaks at 2855 and 2925 cm^{-1}. The organic impurities in this boehmite sample result from the method of preparation based on the hydrolysis of alkoxides of aluminium in water. Three bands are recognized in the hydroxyl-stretching region of both the naturally occurring and synthetic boehmite. The synthetic boehmite displays bands at 3567, 3344, and 3112 cm^{-1} for the 200°C spectrum. The natural boehmite shows bands at 3478, 3319, and 3129 cm^{-1}. The infrared emission band positions differ from the infrared absorption data due to their overlap and broadness (Table III). The two emission bands at 3344 and 3112 cm^{-1} of the synthetic boehmite and the two emission bands at 3319 and 3129 cm^{-1} for the natural boehmite correspond to the two infrared absorption bands for the synthetic boehmite at 3283 and 3096 cm^{-1}. In contrast the infrared absorption band at 3413 cm^{-1} for the synthetic boehmite is shifted to 3567 and 3478 cm^{-1} in the IES spectra of the synthetic and natural samples at 200°C. Each of the hydroxyl stretching modes shows a strong blue shift upon heating. The band at 3344 cm^{-1} at 200°C shifts to 3471 cm^{-1} at 500°C. After this temperature, the intensity reaches zero as the final stages of dehydroxylation occur. For natural boehmite the band at 3319 cm^{-1} at 200°C shifts

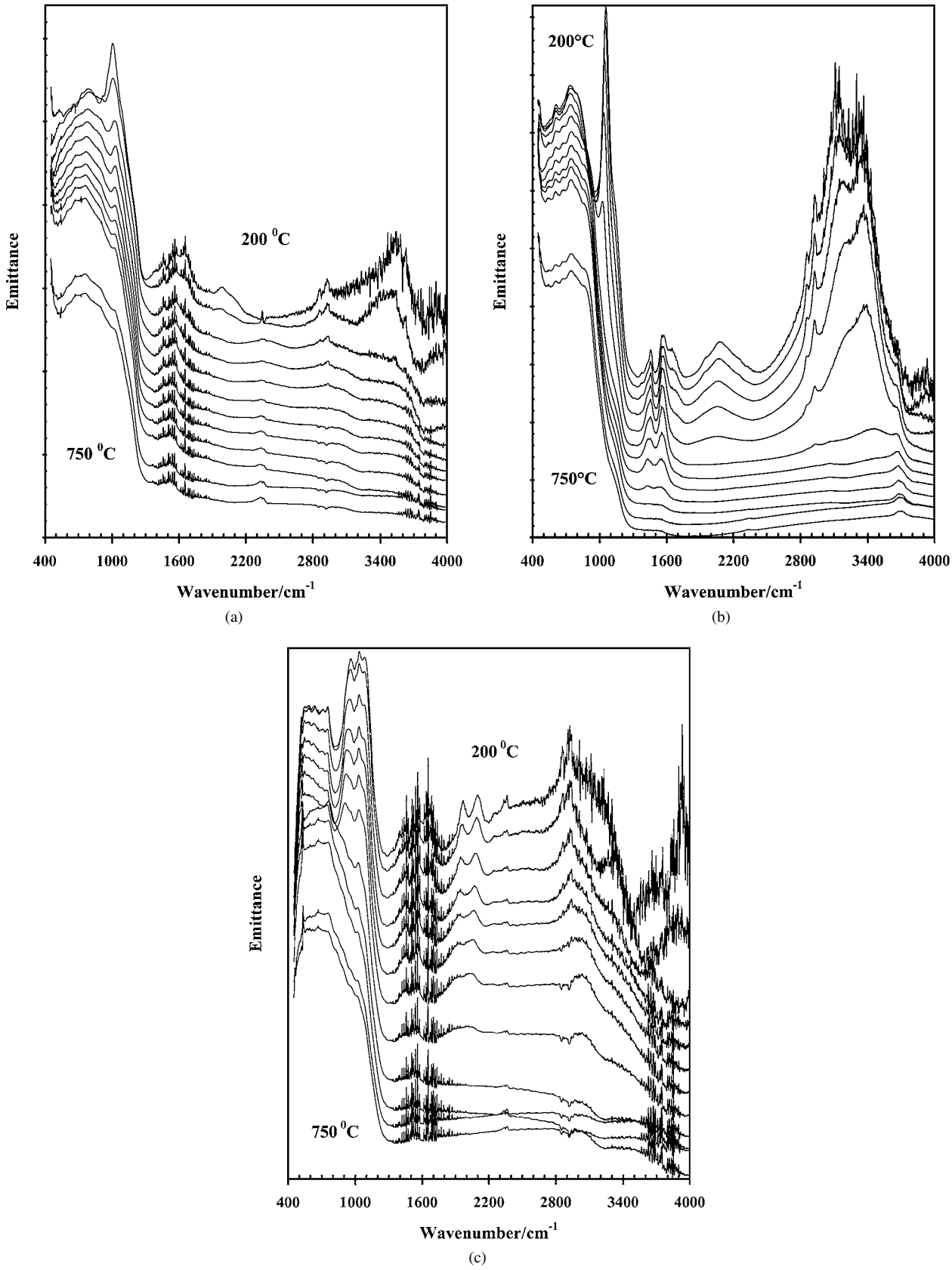

Figure 3 Infrared emission spectra in the temperature range from 200 to 750°C at 50°C intervals of (a) gibbsite 11, (b) synthetic boehmite and (c) diaspore 1151.

to 3417 cm^{-1} at 500°C. The band at 3112 cm^{-1} at 200°C of the synthetic boehmite shifts to 3134 cm^{-1} at 500°C. Similarly, the 3129 cm^{-1} band at 200°C of the natural boehmite shifts to 3209 cm^{-1} at 450°C. The reason for the shift to higher frequencies is attributed to the decrease in hydrogen bonding between adjacent layers. Such a trend has also been observed during the dehydroxylation of kaolinites [39]. As the temperature is increased, the thermal energy is transferred to the hydroxyl vibrational modes. The band around 3567 cm^{-1} decreases in intensity up to 350°C and concomitantly the bands at 3344 and 3112 cm^{-1} decrease in intensity with temperature increase. Above 450°C the hydroxyl stretching bands are no longer observed as the final

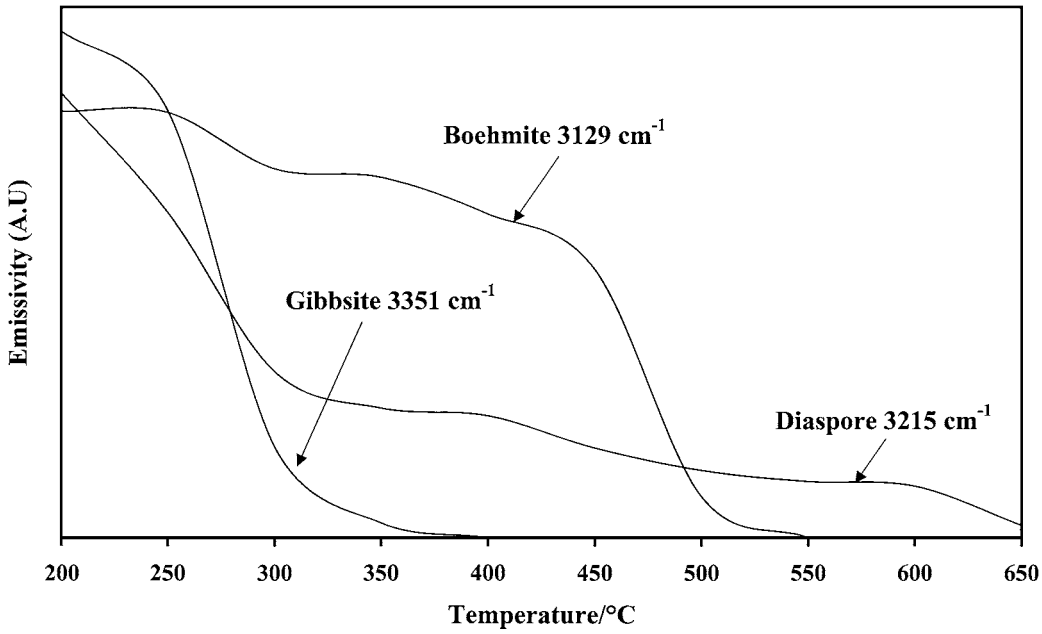

Figure 4 Plot of intensities of characteristic OH-stretching bands of gibbsite (3351 cm^{-1}), boehmite (3129 cm^{-1}) and diaspore (3215 cm^{-1}) as function of temperature.

stages of dehydroxylation are taking place. Each of the hydroxyl stretching bands shows an increase in bandwidth with temperature increase. This indicates that the molecular structure of the boehmite is becoming more disordered during the dehydroxylation process.

As for gibbsite and boehmite the dehydroxylation of diaspore can be followed by the decrease in intensity of the hydroxyl-stretching modes and also by the decrease in intensity of the hydroxyl-deformation modes (Figs 3c and 4). The decrease in the relative intensity of the 3667, 3215 and 2972 cm^{-1} hydroxyl-stretching modes as a function of temperature shows two distinct steps around 350 and 550°C. The latter temperature corresponds well with the temperature of the endotherm 4 in the DTA pattern of diaspore. The decrease in intensity in two steps over two temperature ranges suggests that more than one mechanism is involved in the dehydroxylation process. Above 550°C only a single broad band is observed, which disappears after heating to 600°C. It is suggested that this corresponds with the endotherms 5 and 6 observed around 622 and 650°C in the DTA pattern. As indicated before, diaspore is known to dehydroxylate to alpha-alumina. However, this has not been checked by X-ray diffraction due to the very small amount of sample used in IES measurements (less than 0.2 mg). More information of the newly formed phase can be obtained by looking at the high temperature IES spectrum in the low frequency region.

3.2. The hydroxyl deformation and translation regions

The gibbsite hydroxyl deformation modes are observed in the infrared emission spectra at 1043, 997, and 914 cm^{-1}. The corresponding infrared absorption modes are observed at 1060, 1024, 969, and 914 cm^{-1}. The hydroxyl deformation band is at 1043 cm^{-1} at 200°C shows a considerable blue shift upon heating to 1055 cm^{-1} at 350°C after which little intensity remains in this band. The 914 cm^{-1} band shows a shift towards lower wavenumbers and a decrease in intensity over the temperature range 200 to 300°C. Because of the lack of resolution in this spectral region, particularly at the higher temperatures, the determination of the spectral parameters of this region is difficult. Nevertheless information on the hydroxyl deformation modes of gibbsite may be obtained through the infrared emission spectroscopy. The 778 cm^{-1} band does not shift towards higher or lower wavenumbers throughout the thermal treatment. However, the intensity of this band decreases significantly over the temperature range 200 to 350°C. Therefore this band is ascribed to a hydroxyl translation vibration. Similarly, the bands at 512 and 489 cm^{-1} decreases in intensity over the temperature range 200 to 400°C where no intensity remains in this band. These bands are also assigned to a vibrational mode involving the hydroxyl group.

Boehmites show strong infrared intensity in the 1050 to 1140 cm^{-1} region. Table III reports the hydroxyl deformation modes of the absorption spectra of the natural and synthetic boehmites. Infrared absorption spectra show bands around 1070–1080 and 1135–1160 cm^{-1}. The infrared emission spectra at 200°C show two bands around 1140 and 1057 cm^{-1} for the synthetic boehmite and around 1155 and 1064 cm^{-1} for the natural boehmite. Two Raman bands have been observed at 1049 and 1091 cm^{-1} [37]. There is good agreement between the band positions as determined by the two infrared techniques but not with the Raman technique. No Raman band was observed at $\sim$1160 cm^{-1}, while the Raman band at 1091 cm^{-1} displayed a low intensity. It has to be concluded that the 1140 cm^{-1} emission band is infrared active and Raman inactive. The 1140 cm^{-1} band for the synthetic boehmite shows a strong red shift from 1140 cm^{-1} at 200°C to 1072 cm^{-1} at 400°C. No intensity remains above 400°C. A similar result is obtained for the natural boehmite, where a shift from 1155 cm^{-1} at 200°C to 1127 cm^{-1} at 450°C is

observed. The second hydroxyl deformation band at 1057 cm^{-1} for the synthetic boehmite and at 1064 cm^{-1} for the natural boehmite shows a similar blue shift. The dehydroxylation of the boehmite can be followed by the decrease in intensity of the hydroxyl deformation modes. The hydroxyl deformation modes at 1140 and 1057 cm^{-1} bands show different behavior upon thermal treatment. The 1140 cm^{-1} band intensity is constant with temperature up to 450°C, after which a decrease in intensity to zero is observed. The 1057 cm^{-1} band shows a steady decrease in intensity with temperature until at 450°C a large decrease in intensity is observed. The pattern of this dehydroxylation closely resembles that observed for the hydroxyl stretching frequencies.

The low wavenumber region of the diaspore shows a large number of overlapping bands making the interpretation rather difficult. To band fit broad spectra, bands from the infrared absorption spectrum was chosen as a starting point. Mathematically it is not possible to determine a large number of peaks with an overall broad profile, because there are a large number of possible solutions. In addition, the resolution used for the collection of data was 4 cm^{-1}, which makes the accuracy of a band component analysis rather questionable. Nevertheless, a clear trend in this low wavenumber region can be observed. The overall profile of this region shifts to lower wavenumbers and a decrease in intensity of the bands attributed to the hydroxyl deformation modes at 1102, 1032 and 947 cm^{-1} is observed. Band component analysis of the IES spectrum at 750°C reveals the presence of bands around 1090, 1009, 904, 752, 705, 630, 554 and 458 cm^{-1}, which do not indicate the formation of alpha-alumina but another unidentified alumina phase is formed instead.

4. Conclusions

The decrease in intensity of the gibbsite infrared emission bands around 275°C corresponds well with the temperature of endotherm 2 in the DTA patterns. The decrease in intensity of the 1043 cm^{-1} band around 320°C corresponds reasonably well with endotherm 3. The different endotherms in the DTA patterns correspond to the dehydroxylation of different hydroxyl groups of the gibbsite. The loss of intensity of the hydroxyl stretching bands corresponds to the loss of particular hydroxyls, the outer hydroxyls. The loss of intensity of the hydroxyl deformation vibration may correspond to a different hydroxyl group.

Hence the decrease in intensity occurs at a different temperature. Dehydroxylation of boehmite starts at 250°C and is complete by 450°C. No difference was found between the synthetic and natural boehmite dehydroxylation. This agrees reasonably well with the DTA patterns where the dehydroxylation maximum is observed around 500°C. The temperature difference can be ascribed to the fact that in the DTA a larger sample is used slowing down the diffusion of water from the sample to the atmosphere. The combination of DTA and infrared emission spectroscopy shows that the thermal decomposition of diaspore is complex and more than one mechanism of dehydroxylation is involved. Endotherms were observed at 532, 622 and 650°C. The first endotherm is attributed to the presence of non-substituted diaspore. The effect of Mn substitution caused an increase in the dehydroxylation temperatures. The infrared emission bands of diaspore are observed at similar frequencies to the infrared absorption bands. The DTA patterns of diaspore are significantly different from that of the other alumina phases. The decrease intensity of the hydroxyl stretching bands as a function of temperature mimics the DTA pattern. This paper clearly shows that infrared emission spectroscopy is a strong technique to study the dehydroxylation of different alumina phases such as the oxo(hydroxides) and being able to distinguish between the different phases.

Acknowledgments

The authors thank Greg Cash for his technical assistance with the Infrared Emission Spectrometer. Professor Graeme George is thanked for the use of the infrared emission spectrometer. Sjerry van der Gaast (NIOZ, The Netherlands) is thanked for placing the samples from the collection of van der Marel at our disposal and for the XRD work on these samples. He is also gratefully acknowledged for his helpful discussions. The financial and infra-structural support of the Queensland University of Technology, Centre for Instrumental and Developmental Chemistry is gratefully acknowledged.

References

1. M. L. COSTA, *Expl. Mining Geol.* **6** (1997) 79.
2. L. RINTOUL and P. M. FREDERICKS, *Appl. Spectrosc.* **49** (1995) 608.
3. S. K. SOM and A. K. BHATTACHARYA, *J. Geol. Soc. India* **45** (1995) 427.
4. R. SCHOEN and C. E. ROBERSON, *Am. Mineral.* **55** (1970) 43.
5. A. C. D. NEWMAN, "Chemistry of Clay and Clay Minerals," Vol. 6 (Longman Scientific & Technical, Harlow, UK, 1987).
6. H. W. V. D. MAREL and H. BEUTELSPACHER, "Atlas of Infrared Spectroscopy of Clay Minerals and their Admixtures" (Elsevier, Amsterdam, 1974).
7. H. D. MEGAW, *Z. Kristallogr.* **87A** (1934) 185.
8. A. RAMOS-GALLARDO and A. VEGAS, *ibid.* **211** (1996) 299.
9. Y. I. RYSKIN, in "The Infrared Spectra of Minerals," Vol. Monograph 4, edited by V. C. Farmer (Mineralogical Society, London, 1974) p. 137.
10. T. TAKAMURA and J. KOEZUKA, *Nature* **207** (1965) 965.
11. J. D. BERNAL and H. D. MEGAW, *Proc. Royal Soc.* **151A** (1935) 384.
12. V. A. KOLESOVA and Y. I. RYSKIN, *Optika i Spektrosk.* **7** (1959) 261.
13. W. O. MILLIGAN and J. L. MCATEE, *J. Phys. Chem.* **60** (1956) 273.
14. J. J. FRIPIAT, H. BOSMANS and P. G. ROUXHET, *ibid.* **71** (1967) 1097.
15. W. R. BUSING and H. A. LEVY, *Acta Crystallogr.* **11** (1958) 798.
16. V. A. KOLESOVA and Y. I. RYSKIN, *Zh. Strukt. Khim.* **3** (1962) 680.
17. E. SCHWARZMANN and H. SPARR, *Z. Naturforsch. B* **24** (1969) 8.
18. G. G. CHRISTOPH, C. E. CORBATO, A. HOFMANN and R. T. TETTENHORST, *Clays Clay Miner.* **27** (1979) 81.
19. R. J. HILL, *Phys. Chem. Mineral.* **5** (1979) 179.
20. E. LODDING, in "Thermal Analysis," Vol. 2, edited by R. F. Schwenker and P. D. Gran (Academic Press, New York, 1969) p. 1239.

21. G. ERVIN, *Acta Crystallogr.* **5** (1952) 103.
22. B. G. LINSEN, B. C. LIPPENS and J. J. STEGGERDA, in "Physical and Chemical Aspects of Adsorbents and Catalysts," edited by J. M. H. Fortuin, C. Okkerse and J. J. Steggerda (Academic Press, London, 1970) p. 171.
23. F. FREUND, *Ber. Deut. Keram. Ges.* **44** (1967) 241.
24. C. COLOMBO and A. VIOLANTE, *Clays Clay Miner.* **44** (1996) 113.
25. L. CANDELA and D. D. PERLMUTTER, *AIChE J.* **32** (1986) 1532.
26. V. J. INGRAM-JONES, R. C. T. SLADE, T. W. DAVIES, J. C. SOUTHERN and S. SALVADOR, *J. Mater. Chem.* **6** (1996) 73.
27. H. SAALFELD, *Clay Miner. Bull.* **3** (1958) 249.
28. *Idem.*, *Z. Kristallogr.* **139** (1974) 12.
29. G. ERVIN and E. F. OSBORN, *J. Geol.* **59** (1951) 381.
30. G. C. KENNEDY, *Amer. J. Sci.* **257** (1959) 563.
31. L. ABRAMS and M. J. D. LOW, *Ind. Eng. Chem. Prod. Res. Dev.* **8** (1969) 38.
32. B. C. LIPPENS and J. H. DE BOER, *Acta Crystallogr.* **17** (1964) 1312.
33. S. SOLED, *J. Catal.* **81** (S.) 252.
34. P. A. BUINING, C. PATHMAMANOHARAN, J. B. H. JANSEN and H. N. W. LEKKERKERKER, *J. Amer. Ceram. Soc.* **74** (1991) 1303.
35. A. M. VASSALLO, P. A. COLE-CLARKE, L. S. K. PANG and A. PALMISANE, *J. Applied Spectroscopy* **46** (1992) 73.
36. R. L. FROST, J. T. KLOPROGGE, S. C. RUSSELL and J. L. SZETU, *Appl. Spectrosc.* **53** (1999) 423.
37. *Idem.*, *ibid.* **53** (1999) 572.
38. *Idem.*, *ibid.* **53** (1999) 829.
39. R. L. FROST and A. M. VASSALLO, *Clays Clay Miner.* **44** (1996) 635.

Received 9 April
and accepted 2 November 2001